The overlooked contribution of trees outside forests to tree cover and woody biomass across Europe

Siyu Liu, Martin Brandt, Thomas Nord-Larsen, Jérôme Chave, Florian Reiner, Nico Lang, Xiaoye Tong, Philippe Ciais, Christian Igel, Adrian Pascual, et al.

ECOLOGY

The overlooked contribution of trees outside forests to tree cover and woody biomass across Europe

Siyu Liu[1]*, Martin Brandt[1]*, Thomas Nord-Larsen[1], Jerome Chave[2], Florian Reiner[1], Nico Lang[3], Xiaoye Tong[1], Philippe Ciais[4], Christian Igel[3], Adrian Pascual[5], Juan Guerra-Hernandez[6], Sizhuo Li[1], Maurice Mugabowindekwe[1], Sassan Saatchi[7], Yuemin Yue[8], Zhengchao Chen[9], Rasmus Fensholt[1]

Trees are an integral part in European landscapes, but only forest resources are systematically assessed by national inventories. The contribution of urban and agricultural trees to national-level carbon stocks remains largely unknown. Here we produced canopy cover, height and above-ground biomass maps from 3-meter resolution nanosatellite imagery across Europe. Our biomass estimates have a systematic bias of 7.6% (overestimation; R = 0.98) compared to national inventories of 30 countries, and our dataset is sufficiently highly resolved spatially to support the inclusion of tree biomass outside forests, which we quantify to 0.8 petagrams. Although this represents only 2% of the total tree biomass, large variations between countries are found (10% for UK) and trees in urban areas contribute substantially to national carbon stocks (8% for the Netherlands). The agreement with national inventory data, the scalability, and spatial details across landscapes, including trees outside forests, make our approach attractive for operational implementation to support national carbon stock inventory schemes.

INTRODUCTION

The quantification of wood resources at the national and local scales is a prerequisite for sustainable management of timber resources, habitats, and carbon stocks (*1*–*5*). Local forest management practice and planning relies to an increasing extent on national maps of forests and forest resources, and the accuracy of national carbon stock estimates may be largely improved by inclusion of such maps at the regional and national levels (*6*, *7*).

Most countries focus their inventories and mapping on closed canopy forests (*8*–*10*). Trees outside forests are often associated with scattered dryland trees in arid regions where rainfall is not sufficient for trees to form closed canopies (*11*). However, in northern countries, a substantial part of the woody resource may be growing in hedgerows, gardens, parks, urban areas, grasslands, and agricultural lands. These trees outside forests contribute to carbon storage, provide resources for local communities, modify the local climate, are an important part of habitat networks, affect the hydrological cycle, and thus represent an important economic and social value (*12*–*14*). Many European countries comprise large agricultural and urban landscapes, and the exclusion of trees outside forests from systematic carbon stock assessment potentially implies a bias in national inventories and also affects scientific studies and climate models using only closed forest areas as input (*15*, *16*). For example, reports from the United Kingdom have shown that woody resources provided by trees outside closed canopy forests can exceed those provided by forests (*17*).

Consistent monitoring of both forest and non-forest trees at the national and continental scales remains a challenging endeavor. This is because contemporary forest maps derived from medium-resolution (10 to 30 m) satellite imagery usually miss non-forest trees and do not allow for a clear definition and separation of forest and non-forest areas (*18*). Other maps merge all types of trees under the variable "tree cover" or "forest cover" (*19*, *20*), and it often remains unclear which size classes of trees and shrubs are included and which are excluded. Certain guidelines provide consistent forest definitions, for example, by the United Nations Food and Agriculture Organization (FAO) (*21*). However, the quality and type of data available at the national and continental scales are often not sufficient to apply the guidelines consistently in remote sensing studies. Only few countries provide a high-quality aerial imagery at the national scale that allows for an assessment of all forests and trees (*22*, *23*), but the inclusion of canopy height data derived from airborne Light Detection and Ranging (LiDAR) campaigns is decisive, to separate large trees from shrubs and bushes and to estimate the wood volume, dry mass, and carbon stocks. This is particularly the case for managed forest areas, where small and privately owned lots characterized by different management strategies cause a high spatial heterogeneity within areas considered as closed canopy forest (*5*). High–spatial resolution tree cover maps are not sufficient for a quantification of wood resources as the tree height is unknown. Existing global- and continental-scale canopy height (*24*–*26*) and medium-resolution biomass maps (*27*, *28*) from space-borne sensors largely ignore trees outside forests, providing an incomplete assessment of resources. National canopy height data at a high spatial resolution (<5 m) is expensive and often only available for parts of the country (*29*), if at all. It thus remains unknown to

[1]Department of Geosciences and Natural Resource Management, University of Copenhagen, Copenhagen, Denmark. [2]Laboratoire Evolution et Diversité Biologique, CNRS, UPS, IRD, Université Paul Sabatier, Toulouse, France. [3]Department of Computer Science, University of Copenhagen, Copenhagen, Denmark. [4]Laboratoire des Sciences du Climat et de l'Environnement, CEA/CNRS/UVSQ/Université Paris Saclay, Gif-sur-Yvette, France. [5]Department of Geographical Sciences, University of Maryland, College Park, MD, USA. [6]Forest Research Center, School of Agriculture, University of Lisbon, Lisbon, Portugal. [7]Jet Propulsion Laboratory, California Institute of Technology, Pasadena, CA, USA. [8]Key Laboratory for Agro-ecological Processes in Subtropical Region, Institute of Subtropical Agriculture, Chinese Academy of Sciences, Changsha, China. [9]Airborne Remote Sensing Center, Aerospace Information Research Institute, Chinese Academy of Sciences, Beijing, China. *Corresponding author. Email: sliu@ign.ku.dk (S. Liu); mabr@ign.ku.dk (M.B.)

which extent trees outside forests across the European continent represent a hidden and undervalued resource, as it is the case in the United Kingdom (*17*).

To answer this question and to explore the contribution of non-forest trees to tree cover and woody biomass across Europe, here, we generate continental-scale maps of forests, woodlands, and trees outside forests, including their height at 3-m resolution in 2019, which contains a level of details otherwise only previously accessible from the use of airborne LiDAR surveys. We retrieve these data from cost-efficient nanosatellites available at a daily basis and at a spatial resolution high enough to map large individual trees (>3-m height) using a deep learning approach where a convolutional neural network is learned end to end from airborne LiDAR canopy height reference data across Europe. We trained two deep learning models from PlanetScope optical imagery at 3-m resolution: (i) a segmentation model predicting binary canopy/no-canopy (>3-m height) and (ii) a regression model predicting canopy height. Tree crowns and their shadows are visible in PlanetScope images, representing key features when training deep learning methods to retrieve canopy heights. Furthermore, we use inventory data to convert tree cover and height into aboveground biomass maps including both forest and non-forest tree biomass, forming the basis for quantifying and comparing forest and non-forest tree resources across European countries. We further apply the model trained in Europe to the boreal and temperate zones of North America to test the scalability of the approach to different areas evaluated on independent datasets.

RESULTS

A canopy height map at 3-m resolution for Europe

We used 0.7 million km^2 of canopy height data from airborne LiDAR available for Denmark, The Netherlands, Switzerland, Estonia, Spain, Finland, and Wales (fig. S1B) to train a deep learning model and predict tree height and binary tree cover from PlanetScope imagery in 2019 at 3-m resolution for all Europe (10 million km^2; Fig. 1). The training data cover boreal, temperate, and Mediterranean areas (fig. S1A). Model performance was evaluated on 10,000 km^2 of randomly sampled airborne LiDAR data (organized as 1 km–by–1 km tiles), which was not used for model training and hyperparameter optimization (Fig. 2 and fig. S2).

At the pixel level, canopy height was predicted with a low random error for boreal [root mean square error (RMSE) = 4.33 m and relative RMSE (rRMSE) = 21.7%] and temperate zones (RMSE = 5.06 m and rRMSE = 27.8%), but the diverse tree structure of Mediterranean regions results in a higher uncertainty (RMSE = 6.44 m and rRMSE = 32.2%), observed as a more severe underestimation at higher canopies (>30-m height) (Fig. 2A), which can be partially explained by the uneven distribution of the validation data, with a lower number of points for higher canopies (Fig. 2B). Aggregating tree cover and height to 1 km–by–1 km grids, we found that the overall systematic bias (see Materials and Methods for equation) between our PlanetScope predictions and LiDAR data for areas outside forests, here defined as trees that we mapped in the "urban" and "cropland" classes using a global land cover and land use (GLCLU) dataset (*30*), was −1.6% for canopy height and −2.6% for canopy cover. For closed canopy forests, here defined as areas mapped as forest in the GLCLU dataset, the bias was −1.2% for canopy height and +0.4% for canopy cover (Fig. 2C). When comparing two global canopy height products with airborne LiDAR-derived canopy cover and height, the systematic bias was high, particularly for trees outside forests: Here, the bias for canopy height and cover was +15.4 and +231.2%, respectively, for a fused Sentinel-2– and spaceborne LiDAR [Global Ecosystem Dynamics Investigation (GEDI)]–based map at 10-m resolution (*26*), while it was −31.3 and −95.8% for canopy height and cover, respectively, for a Landsat- and GEDI-based map at 30-m (Fig. 2D) (*24*).

Quantification of tree cover outside forests across Europe

To refine the forest versus non-forest area definition in relation to our dataset, we used the FAO definition (*21*) to separate forests from non-forest trees. Here, we aggregated our PlanetScope-based tree cover and tree height maps into 0.5-ha grid cells. Following the FAO definition, woody vegetation in 0.5-ha grids where the canopy cover of trees taller than 5-m height exceeded 10% and where the land use was not agricultural land or urban according to (*30*) was considered as forest. Note that the FAO definition includes areas of trees that potentially can grow above 5 m, which cannot be resolved for our map. Conversely, trees in 0.5-ha grids where the cover of trees taller than 5 m was below 10% or where the land use was urban or agricultural land were considered as trees outside forests. Following these definitions, we find that forests cover 377 million ha, equivalent to 28% of the total land area shown in Fig. 1. The canopy cover of trees outside forests represents 16.1 million ha, which is 1% of the total land area and 4% of the total tree cover. The precise percentage of cover due to trees outside forests depends on a number of factors including land cover maps and spatial resolution of the product (fig. S4).

To analyze the spatial distribution of both forest and trees outside forests, we aggregated our results at the country scale (Fig. 3, A and B) and to 1° units (Fig. 3C). Results show that almost half of all countries (44%) have a national forest cover between 30 and 45%, and trees outside forests contribute less than 5% to the total tree cover for about half (53%) of the countries. Northern Europe is mostly covered by forest with limited trees cover outside forests: Finland, Slovenia, and Sweden have the highest percentage of national forest cover (66, 63, and 61%, respectively) and the lowest contribution of tree cover outside forests to the total tree cover (1.8, 2.8, and 1.9%, respectively). On the contrary, the least forested countries (United Kingdom, 12%; The Netherlands, 12%; and Denmark, 15%) have the highest contribution of tree cover outside forests to the total tree cover (22.1, 24.5, and 19.5%, respectively). The highest contribution of trees outside forests at 1° grid scale is found in Western Europe along the coast and Southwestern Europe (up to 40% in Fig. 3, C and E) where agricultural and residential areas are concentrated and forest coverage is consequently low. The histogram results show a roughly even distribution of forest cover percentage, with most of the trees outside forests accounting for less than 10% of the total tree cover (Fig. 3, D and E). For forest areas, our results compare well with the national FAO statistics (fig. S5). Differences can be explained by the slightly different definitions of forests. For example, the FAO definition includes areas with shorter trees that can grow taller than 5 m, such as reforestation and afforestation, which were excluded in our map.

We then quantified tree cover for different land use/cover classes (Fig. 3F), by aggregating our data into 0.5-ha grids. For Europe as a whole, we identify 15.5 million ha of trees located outside the "forest" class of GLCLU, in which half of them are found in

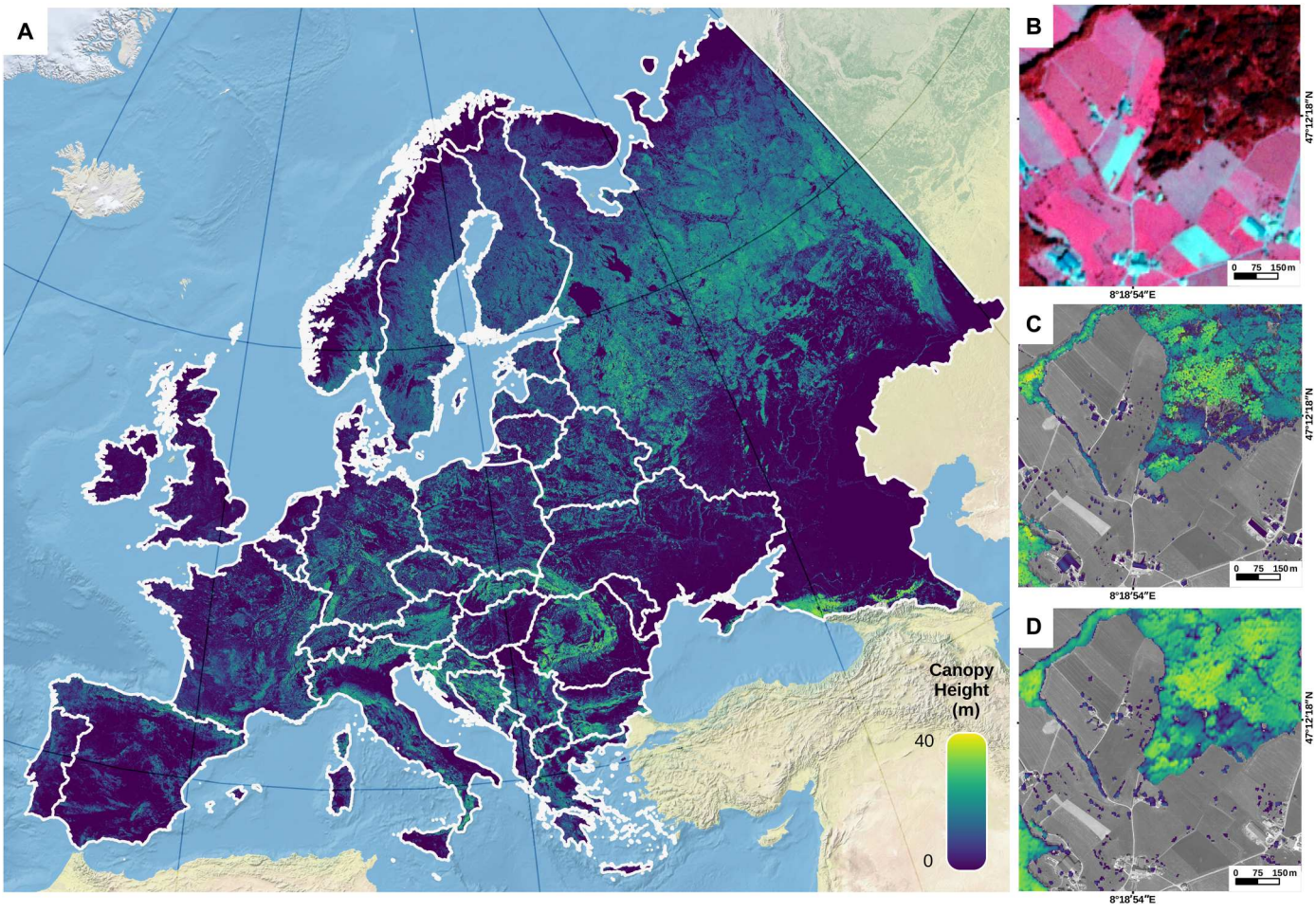

Fig. 1. PlanetScope-based canopy height map for Europe at 3-m resolution for 2019. (**A**) Spatial distribution of average canopy height aggregated to 1-km resolution for visualization purpose. (**B**) PlanetScope imagery example in Switzerland displayed as near-infrared, red, and green false color composite. (**C**) Corresponding canopy height models (CHMs) from airborne LiDAR at 0.5-m resolution. (**D**) Same area as (B) but showing the PlanetScope-based canopy height prediction at 3 m. The land base maps in (C) and (D) are from Google Maps satellite imagery (Imagery 2022 CNES/Airbus, Landsat/Copernicus, Maxar Technologies, Map data 2022). The land and ocean base map in (A) is from www.naturalearthdata.com.

"dense short vegetation" (hereafter referred to as grassland), with a median (25 to 75 percentiles) canopy cover of 7.2% (2.1 to 19.2%). Urban areas have on average the highest canopy cover (12.7%; 4.5 to 26.9%), with an aggregated tree cover of 5.05 million ha. Tree cover of a total of 2.67 million ha is found in cropland with a rather low canopy cover percentage per hectare (4.6%; 1.4 to 12.2%). Detailed statistics are found in table S1.

Quantifying aboveground biomass across Europe

To quantify the woody resources into aboveground biomass, we used plot-based National Forest Inventory (NFI) data (fig. S13) and airborne LiDAR canopy height model (CHM) data from Denmark (*31*) to establish allometric relationships between aboveground biomass and canopy height, both averaged at the plot level (n = 11,296). Separate relationships were derived for broadleaf forest (n = 7232; bias = −8.8%), coniferous forest (n = 3768; bias = −6.8%), mixed forest (n = 7536; bias = −9.9%), and plots with sparse tree cover (n = 409; bias = −5.9%) (fig. S6) using a previously published forest-type map from 2018 (*32*) for the separation (see Materials and Methods). We aggregated aboveground biomass to the hectare level (100 m by 100 m) including both forest and non-forest trees (Fig. 4). The overall uncertainty is the combined uncertainty due to the canopy area and height prediction and to the height to biomass conversion and was quantified by comparing our final aboveground biomass product (after application of the allometric conversion on PlanetScope canopy height and cover data) with field measured biomass from the Danish (n = 3451) and Spanish (n = 1706) NFI data at the plot scale and the country scale (n = 30). At the plot scale, the correlation was moderate [correlation coefficient (r) = 0.53 and bias = −23% for Denmark; and r = 0.50 and bias = −25% for Spain] (fig. S7, C and D), which was expected because of a large uncertainty related to both satellite and field data, such as geolocation and image quality errors. These errors were found to be not systematic, as demonstrated by a comparison of statistics aggregated to the country scale, both from NFI and satellites. Here, the systematic bias was −10% (underestimation) for Denmark and +5% (overestimation) for Spain, which can be explained by the fact that clear-cut areas and young tree plantations are part of the national statistic but are

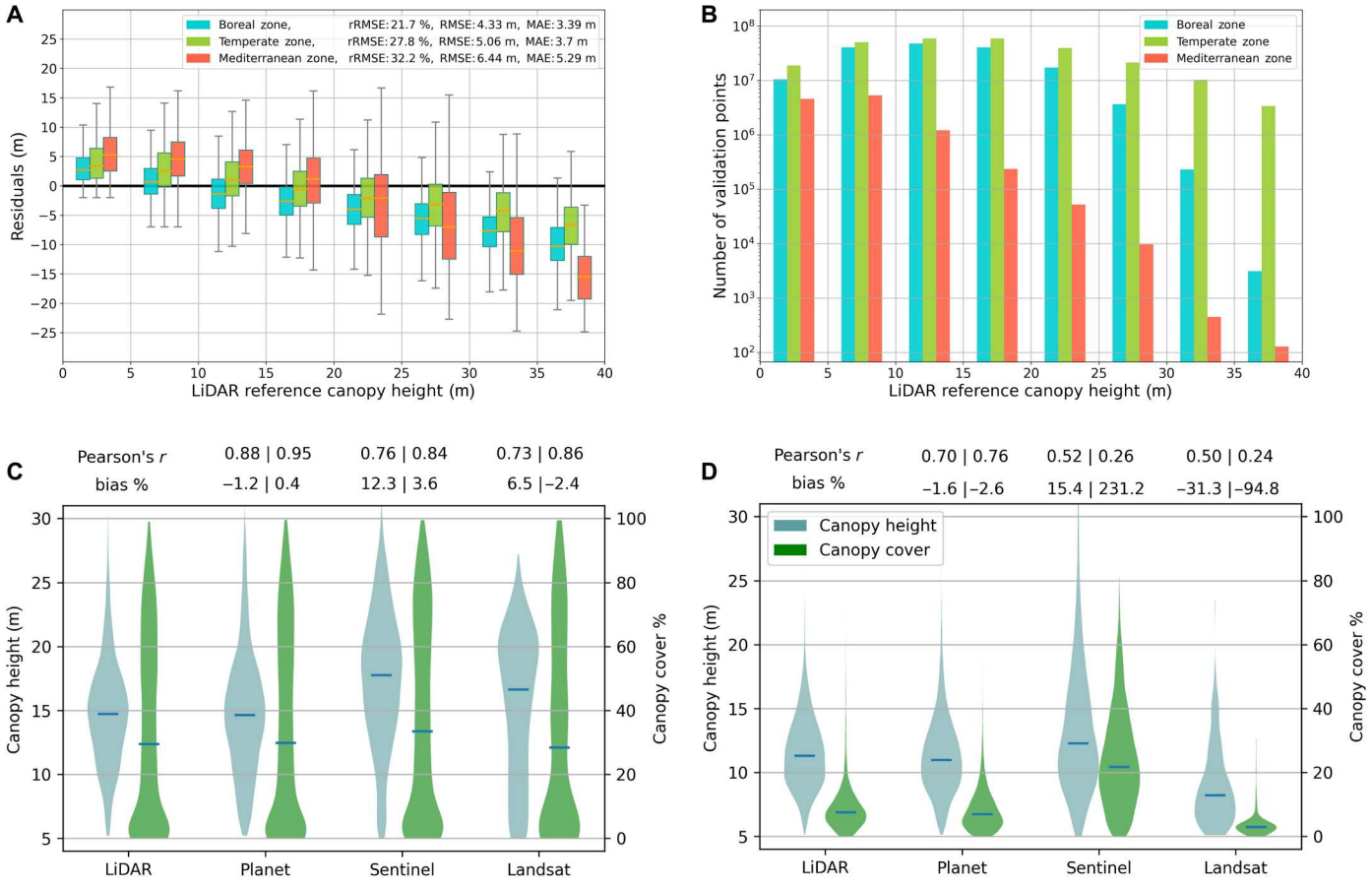

Fig. 2. Evaluation of canopy height and cover. (**A**) Residuals at 3 m by 3 m between aerial CHM and our PlanetScope-based predictions, grouped in 5-m height intervals. (**B**) Number of evaluation points used in (A). See fig. S1 for biome zones (*62*). (**C** and **D**) Violin plots of canopy height and canopy cover for airborne LiDAR-based CHMs, PlanetScope predictions (this study), a Sentinel-2–based product from (*26*), and a Landsat-based product from (*24*) aggregated to 1 km–by–1 km samples (that were not used for training and parameter optimization) divided into forest areas (n = 4772) (C) and non-forest areas (n = 5228) (D). Forests and non-forest areas are defined by the GLCLU dataset. Two-tailed Pearson correlation and bias are calculated between the airborne LiDAR-based CHM samples and the other products (all aggregated to 1 km by 1 km). See corresponding scatter plots in figs. S2 and S3. The horizontal blue line is the median and the violins show the data distribution. Pixel-level height distribution of trees outside forests is shown in fig. S12. See Materials and Methods for the bias calculation.

not mapped in our product. The bias was +7.6% over 30 countries with a Pearson correlation of 0.98 (Fig. 5D and fig. S9A). The relatively even distribution of the error across countries demonstrates the transferability of the approach beyond Denmark. A previously published state-of-the-art biomass map from (*28*) had a larger bias of +17.3% when compared against country statistics. Aggregated to 1 km–by–1 km scale, our map compares reasonably well with existing products (fig. S8) (*27*, *28*, *33*), with the advantage of including information on non-forest trees (Fig. 4).

Following the FAO forest definition, European forests have an overall aboveground biomass of 35.2 Pg, and trees outside forests represent only 0.8 Pg, which is a proportion of 40:1. By further aggregating our biomass maps into forest types and biomes, we found that broadleaf and coniferous forests in the temperate zone have a biomass density of 140.4 (84.8 to 195.8) Mg/ha and 110.1 (50.4 to 174.6) Mg/ha, respectively (Fig. 5, A and B). Using the global land use and land cover class (GLULC) classification, our results reveal that trees in urban areas have a total biomass of 0.22 Pg with a median biomass density of 5.6 (2.5 to 13.2) Mg/ha, trees in croplands have 0.11 Pg with a median biomass density of 3.8 (1.9 to 8.5) Mg/ha, and trees in grassland have 0.29 Pg with a median biomass density of 4.6 (2.1 to 11.1) Mg/ha. Overall, 44.6% of the tree biomass outside forests is found in grasslands, 34.0% in urban areas, and 16.2% in croplands (Fig. 5C).

At the country scale, we ranked the top five countries having the highest contribution of non-forest trees for different GLULCs to the national biomass stocks. Ireland was ranked first, with 16.5% of the tree biomass located outside forests, followed by the United Kingdom (14.8%), The Netherlands, which has 8.2% of its national biomass located in urban areas, and Denmark (9.7%) (Fig. 5C). We found a negative relation between the total tree cover percentage and the biomass contribution by trees outside forest (Table 1). The Netherlands stands out with both the highest tree cover outside forest (24.6%) and a high biomass contribution in percentage (12.2%). France has the largest total biomass (2388.2 Tg), while the tree biomass outside forests is only of 77.2 Tg.

Beyond Europe

To test the scalability of our approach, we applied the tree cover segmentation and canopy height prediction to the boreal and

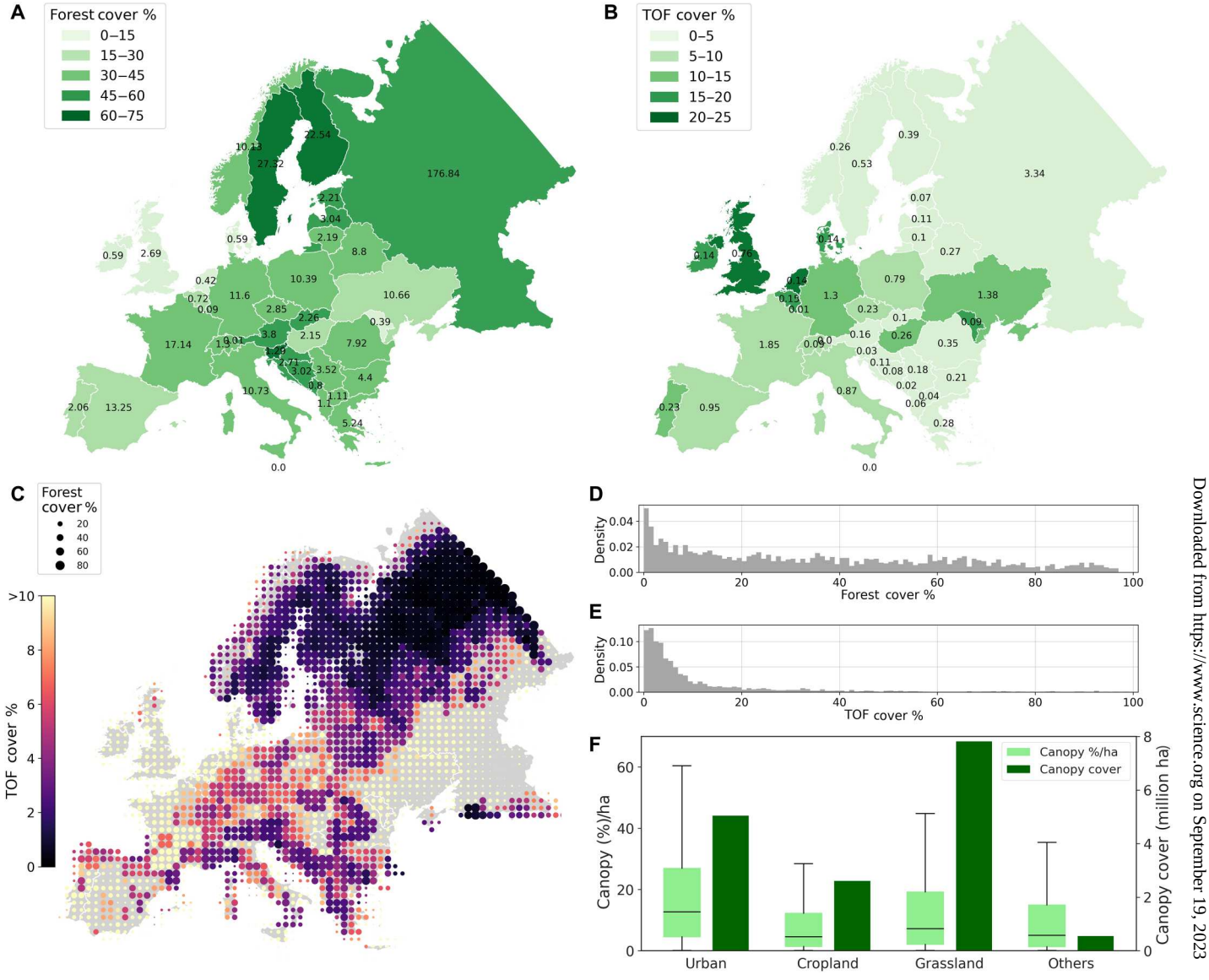

Fig. 3. Quantification of tree cover outside forests across Europe. (**A**) Total forest area in million hectares and the percentage of surface area at the country scale. (**B**) Trees outside forest (TOF) area in million hectares and the percentage of total tree cover at the country scale. (**C**) Percentage of forest (size of the circle) and TOFs (color of the circle) cover for 1° by 1° grids. (**D**) Forest cover percentage histogram at 1° by 1° as shown in (C). (**E**) TOF cover percentage histogram at 1° by 1° as shown in (C). (**F**) Canopy cover of different GLCLU landscape types: The boxplots show the canopy cover percentage per hectare, and the bars denote the total canopy cover area per class. For the boxplots, the start of the horizontal line represents the minimum value; vertical lines represent first quartile, median, and third quartile values, respectively; and the end of the horizontal line represents the maximum value.

temperate zones of North America and tested the performance with a fully independent LiDAR dataset (1000 km^2 at 1-m resolution) that was never seen during training and parameter optimization (Fig. 6). Errors were found to be comparable to the European test datasets if aggregated to 1 km–by–1 km samples [coefficient of determination (R^2) = 0.71, bias = −15.7%, and rRMSE = 20% for height regression; and R^2 = 0.88, bias = +2%, and rRMSE = 28.6% for tree cover segmentation]. At 3 m by 3 m, the overall RMSE was higher than in Europe (6.5 m). Note that a conversion to biomass would requires region-specific calibrations with local field data, which is beyond the scope of this study.

DISCUSSION

Trees outside forests in Europe have always been overlooked, and only the United Kingdom has so far conducted a systematic assessment of their resources (*17*). They conclude that, in many areas, the carbon stored in non-forest trees exceeds the forest carbon stocks, which would imply that current carbon stock assessments include a large bias.

Here, we show that, at the continental scale, trees outside forests do not play a critical role for the national aboveground carbon stocks of many Northern European countries. However, this is because of the dominant role of forest landscapes. We found the total amount of carbon in non-forest trees (0.37 Pg) is about the

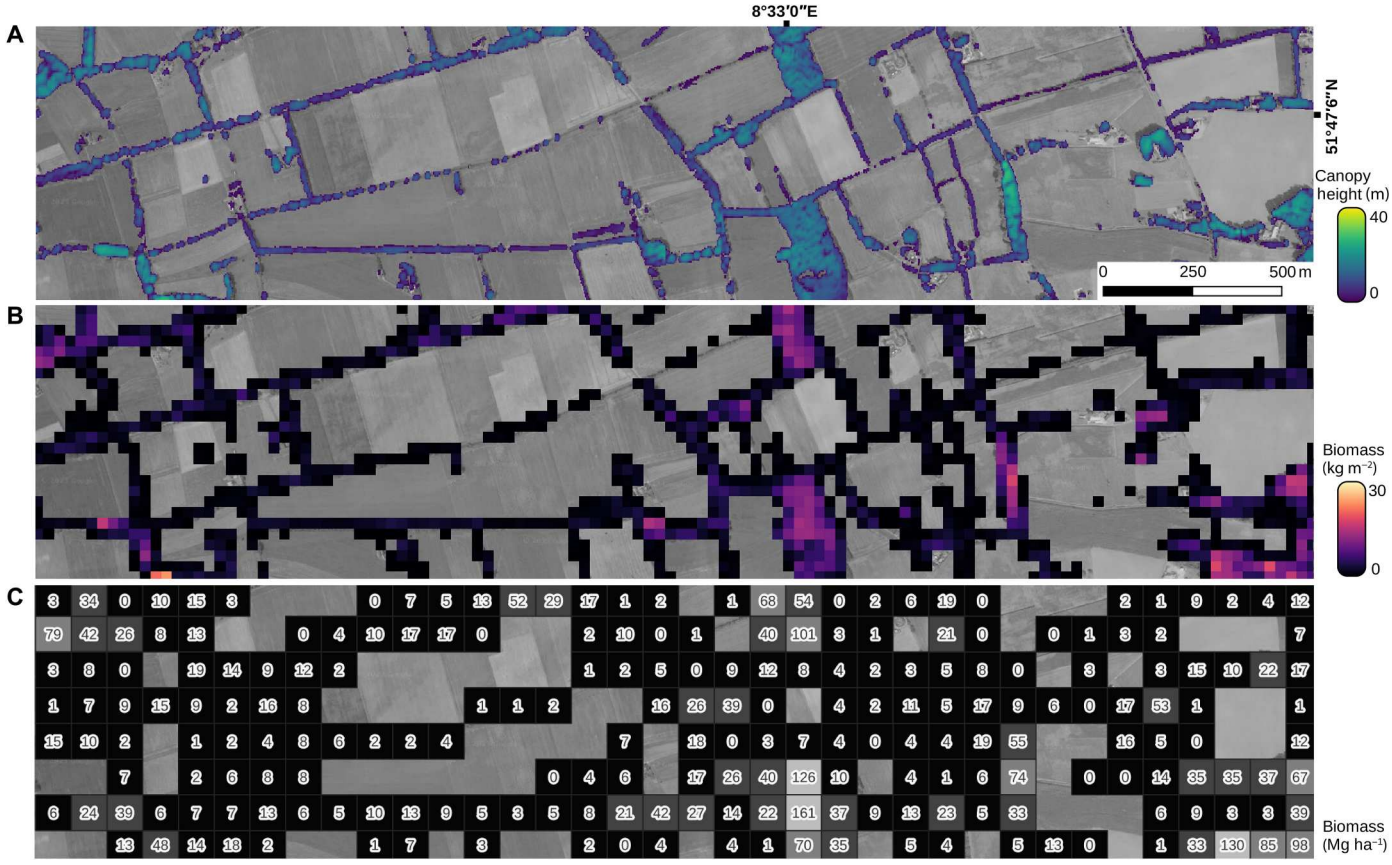

Fig. 4. Aboveground biomass estimation using PlanetScope. (**A**) PlanetScope-based canopy height map at 3-m resolution. (**B**) Biomass density estimation based on (A) derived from allometry equation at 30 m by 30 m in kilograms per square meter. (**C**) Biomass density per hectare aggregated from (B) in megagrams per hectare. The base map is from Google Maps satellite imagery (Imagery 2022 CNES/Airbus, Landsat/Copernicus, Maxar Technologies, Map data 2022).

Table 1. Country statistics of tree cover and biomass. Ten example countries sorted by the total tree cover percentage. Full country statistics are provided in table S1. The class trees outside forests were defined following the FAO definition.

Country	Total tree cover (% of country)	Tree cover outside forests (% of total)	Total biomass in Tg	Tree biomass outside forests in Tg (% of total)
Ireland	10.5%	19.7%	36.65	3.24 (8.8%)
United Kingdom	14.1%	22.1%	264.29	26.29 (9.9%)
The Netherlands	14.8%	24.6%	47.32	5.79 (12.2%)
Denmark	16.9%	19.5%	63.47	4.74 (7.5%)
Ukraine	20.1%	11.4%	1534.2	53.2 (3.5%)
France	34.6%	9.7%	2388.2	77.2 (3.2%)
Germany	36.1%	10.0%	2264.3	65.4 (2.9%)
Italy	38.6%	7.5%	1501.3	37.6 (2.5%)
Estonia	50.3%	3.0%	259.3	2.7 (1.0%)
Finland	67.8%	1.7%	1726.2	9.76 (0.6%)

same (0.30 Pg) as was previously found in billions of African dryland trees over the arid and semiarid African Sahel, also with comparable carbon density values (1.9 to 2.8 Mg/ha versus 1.5 Mg/ha in semiarid area) (*34*). This implies that trees outside forests are not only an overlooked resource in dryland area (*11*), but they are equally important for European landscapes.

We also found that there are several countries and regions where the tree cover outside forests exceeds 20% of the national tree cover (Fig. 3B). In particular, urban areas can have a relatively high tree cover, and their contribution to the national aboveground biomass can be considerable. In addition, at the subnational scale, many areas have a large proportion of trees outside forests (Fig. 3C), and excluding them causes a substantial bias in local carbon budgets. Moreover, trees outside forests are not only valuable for their carbon stock, and a systematic identification of their location could be an integral part of annual monitoring and planning schemes related to biodiversity, microclimate, habitats, landscape values, and hydrological cycles (*12*, *13*).

Our canopy cover, height, and biomass products provide a level of detail that was previously only possible with airborne data from LiDAR, which are costly and rarely available at the national level. Airborne LiDAR-derived maps of woody resources are not available at the continental scale, and spaceborne LiDAR from GEDI (*35*) is only available at a point scale and not over multiple years. Furthermore, GEDI and also the soon-to-be-launched BIOMASS mission

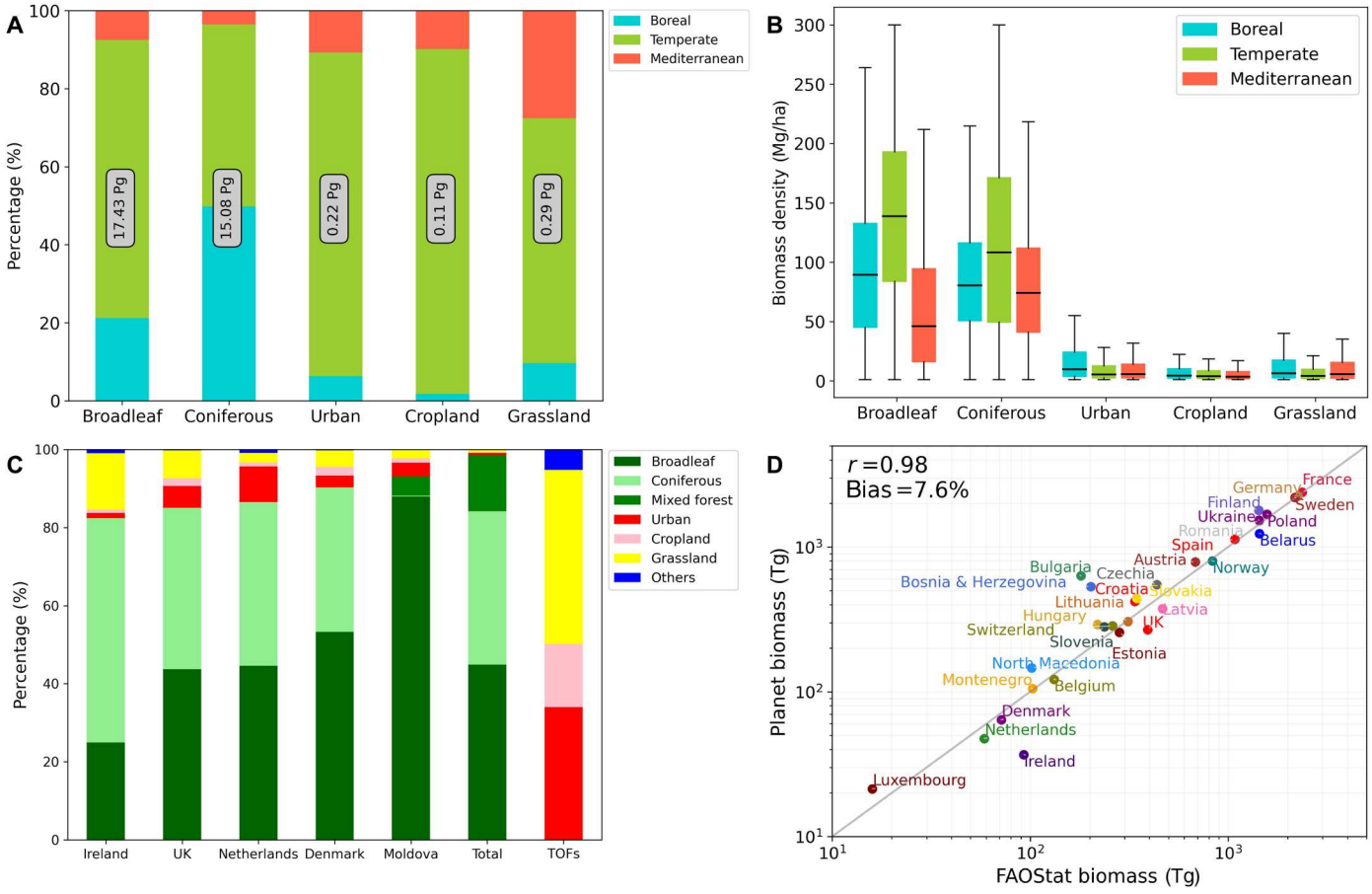

Fig. 5. Aboveground tree biomass across tree types, land use/cover and countries. (**A**) Total tree biomass for different forest and land use/cover types; the color reflects the biomes. (**B**) Same as (A) but for biomass density. (**C**) Top five countries with the highest contribution of non-forest tree biomass to the national biomass stocks, as well as distribution of biomass among land use/cover classes. (**D**) Country-level biomass comparison between PlanetScope-based estimations and FAO statistics (*5*). Forests are defined by GLULC and divided into broadleaf and coniferous using a previously published forest-type map from 2018 for countries in the European Economic Area (EEA) and the PROBA-V forest-type map (2019) for countries outside the EEA (Belarus, Moldova, Russia, Ukraine) (*32*). For more countries, see fig. S9.

do not cover the northern parts of the world (*36*). Previous studies combined sparse GEDI data with Landsat (*24*) or Sentinel-2 (*26*) to generate global-scale canopy height maps, and, although these perform well in forests, they have a large bias in non-forest areas (Fig. 2, C and D). Moreover, the major strength of deep learning with 3-m resolution nanosatellite imagery lies in the fact that the model can learn features from the visible tree crown structure, which is often less clear in Sentinel-2 (10-m) or Landsat (30-m) images.

Our maps could be operationally integrated in national carbon stock inventory schemes. First, the spatial resolution allows to identify individual tree crowns and makes it possible to align the satellite image with field plot data, which can be useful to reduce variances when upscaling plot data on, e.g., carbon stocks to the national scale. Using different canopy height-to-biomass conversions for different forest and non-forest types account for the bias caused by the forest understory, which is undetected by classic aerial surveys. Aggregating our biomass maps to the national scales shows a good alignment with national NFI statistics (bias of 7.7% overestimation for 30 countries) (*5*), although NFI plot-level data were only available for Denmark. Second, while the imagery is not free of charge, it is cheaper than aerial imagery, making it feasible to be acquired annually at the national scales. The daily global coverage facilitates cloud-free mosaics of different periods of the year, and, once a model is trained, it has potential to be applied each year on an operational basis without further need of LiDAR data. Our example of North America demonstrates the geographical robustness of our models over trained biomes, but canopy height estimations in dry and tropical areas require further work. Third, LiDAR and aerial imagery differ between countries with regard to spectral, spatial, and temporal resolution, making it difficult to create biomass maps that are consistent between countries and years at the continental scale. Although this was not demonstrated in this study, PlanetScope-based maps have a certain consistency in space and time (*37*, *38*), allowing for large-scale and multiyear biomass assessments. Fourth, integrating trees outside forests in national inventories is not only interesting from a carbon stock perspective but also allows to quantify a variety of ecosystem services provided by these trees. A previous study used submeter LiDAR and aerial images to quantify the tree cover outside forests in Denmark, yielding the same proportion as this study (20%) (*39*), confirming the reliability of the PlanetScope-based map for the mapping of

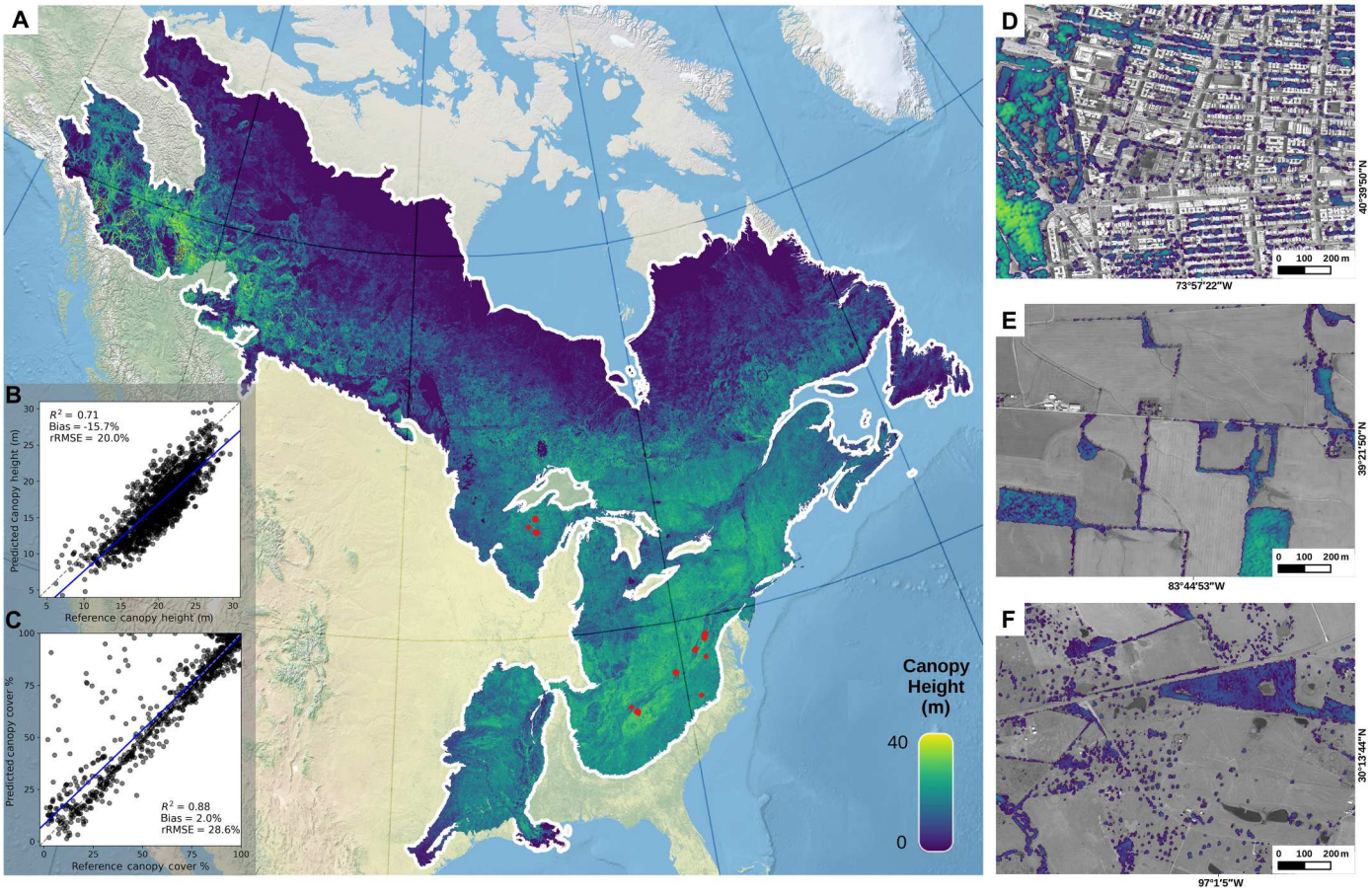

Fig. 6. Canopy height estimation for the boreal and temperate zones in North America. (**A**) Canopy height aggregated to 1-km resolution. (**B**) Scatter plot of canopy height from aerial CHM and PlanetScope predictions in test areas [red boxes in (A)] using canopy height averaged over 1 km–by–1 km sample sites (n = 1036). (**C**) Same as (B) but for canopy cover percentage. (**D** to **F**) Zoom-in examples of canopy height predictions in urban (D), cropland (E), and grassland (F) areas at 3-m resolution. The land base map in (D) to (F) is from Google Maps satellite imagery (Imagery 2022 CNES/Airbus, Landsat/Copernicus, Maxar Technologies, Map data 2022). The land and ocean base map in (A) is from www.naturalearthdata.com.

non-forest trees. For the United Kingdom, we found the fraction of urban trees outside forest cover to be 20.2%, which is in general agreement with the 16.5% reported in the U.K. NFI (*17*). Moreover, the overall forest cover percentage found for the United Kingdom (12%) is in line with previous reports (*17*, *40*, *41*).

A drawback of the presented method is the requirement of large amounts of airborne LiDAR for training and validation, as well as NFI data for converting canopy cover and height into biomass, which now limits the applicability primarily to the Global North. Although our map has shown robustness across Europe, the generalization to North America yields comparable results when aggregated at 1-km resolution, but the performance at the 3-m pixel level drops. Nevertheless, fine-tuning on some reference data from a previously unknown region of interest will likely close the performance gap. The conversion of height and cover into biomass can potentially be improved by more region-specific field data, but using allometric equations from the Spanish NFI data showed that the equations established from the Danish NFI data are robust (see Materials and Methods). In semiarid regions, small trees form a complex matrix of low vegetation, representing more challenging conditions for accurate predictions of the deep learning–based model. We confirm this with higher error values in the Mediterranean zone (Fig. 2A and fig. S3), where our map should be used with caution. The inclusion of additional LiDAR data from mixed vegetation types, as well as semiarid and arid regions, will improve future versions of the model. Acknowledging these current shortcomings, recent development of state-of-the-art methods from the field of machine learning combined with cost-efficient nanosatellite imagery with a spatial resolution below 5 m opens a previously unknown research avenue toward improved monitoring of national tree resources, both in and outside forests. This could allow the systematic integration of trees outside forests into local, regional, and global carbon budgets, national inventories, climate models, and carbon credit programs and improve the management of tree resources in countries characterized by predominantly non-forest landscapes. While this study concludes that the impact on national statistics of most European countries will not be marked due to the dominant role of forests, we also show that the amount of carbon stored in European non-forest trees is comparable to dryland areas, where trees outside forests are dominating the landscapes (*34*).

MATERIALS AND METHODS

Summary

We used CHMs from airborne LiDAR data across Europe to train two deep learning models: a segmentation model predicting binary canopy/no-canopy (for trees taller than 3-m height) and a regression model predicting canopy height, both from PlanetScope optical imagery at 3-m resolution. The canopy map was used as a mask, and canopy height was only predicted within areas identified as tree cover. We included a GEDI- and Sentinel-2–based canopy height map from (*26*) as an additional model input, in both the training and prediction processes, providing a priori knowledge on the height distribution of forest areas. We observed that this improved the underestimation of tall forest trees and that, in case of temporal or spatial mismatches (e.g., clear-cuts and trees outside forests), the prediction followed the PlanetScope image overruling the information from the GEDI/Sentinel-2 map. Here, it is important to mention that the map from (*26*) severely overestimates trees in sparsely vegetated areas, which, however, did not affect our result because we applied a binary canopy map at 3 m as mask (fig. S4). We used Danish NFI data to establish allometric relationships between plot-based aboveground biomass and height (>1.3 m) from aerial CHMs averaged over the field plot. The relationship between canopy height and biomass was then used to convert canopy height and cover predicted from PlanetScope imagery into biomass at 30-m resolution (same as NFI plot), which was lastly aggregated to the hectare level. We did not use the field measured height but the average vegetation height from the LiDAR data per plot because it comes closest to our predicted height. We also did not use PlanetScope predicted height because of alignment uncertainties with the field plots at 3-m resolution. The lack of publicly available GPS-referenced field plots covering the entire continent makes it impossible to train a model that can predict biomass directly from PlanetScope imagery.

Data

PlanetScope imagery

We used PlanetScope imagery from Planet Labs available via a research license. The images are available daily for the entire globe with approximately 3-m pixel resolution and four multispectral bands: red, green, blue, and near infrared. We generated yearly 1° by 1° tiles of mosaics from around 100,000 image scenes for the study area from 2019. Each mosaic tile consists of roughly 100 high-quality cloud-free scenes and was selected within a time window according to the Moderate Resolution Imaging Spectroradiometer (MODIS) phenology product (*42*). The selected time window started 25 days before "senescence" and ends 10 days before "midgreendown," which reflects late summertime in Europe, where all woody vegetation still has green leaves and visible crown structure. For areas with frequent cloud cover, the time window was progressively extended toward earlier dates until the whole tile was fully covered with scenes. To reduce differences resulting from the mosaicking scenes collected from different sensors and times, we applied a histogram matching to Landsat and Sentinel-2 surface reflectance images from the same date range to produce homogeneous mosaics (*38*).

Airborne LiDAR canopy height maps

We collected publicly available airborne LiDAR CHM data in Europe and the United States, with full country coverage for Denmark (0.4 m-resolution merged from 2016 to 2021, in total 43,000 km^2), Estonia (1-m resolution from 2011 to 2017, in total 45,000 km^2), The Netherlands (0.2-m resolution from 2018, in total 41,000 km^2), and Spain (2.5-m resolution from 2008 to 2015, in total 500,000 km^2). Other samples were available for patches in Finland (1-m resolution from 2019, in total 50,000 km^2), Switzerland (0.5-m resolution merged from 2017 to 2020, in total 20,000 km^2), and Wales (1 m-resolution from 2015, in total 10,000 km^2) (fig. S1B). Some data were provided as CHM, others as raw cloud points, which were converted to Digital Terrain Model (DTM) and Digital Surface Model (DSM) used to calculate CHMs via LAStools (*43*). CHM data represent the top canopy height in the pixel area but, sometimes, include the height from buildings and short herbaceous and bush vegetation. Here, we used the building footprints from Microsoft (*44*) and Open Street Map (*45*) to mask buildings. We further visually compared PlanetScope imagery and the corresponding CHM and decided for a 3-m height threshold to separate tree crowns from shrubs, bushes, and grasses. Woody plants below this threshold were not clearly visible in the PlanetScope images.

Training sample generation

To adjust airborne CHM with PlanetScope images, we reprojected the PlanetScope imagery to match the aerial data Universal Transverse Mercator (UTM) projection and resampled the aerial CHM to the spatial resolution of PlanetScope data (3 m) by reserving maximum values (filling small gaps in forests in the aerial CHM, which are not visible in PlanetScope imagery). We applied a weighted sampling strategy to the aerial CHM data, according to collection year, mean height, tree cover percentage (area > 3 m), forest type [coniferous or broadleaf (*32*)], and dominating land use/cover classes, to control the training data distribution fitting into the model and to minimize possible mismatches between data sources caused by acquisition time differences (fig. S11). The final dataset contains 100,000 samples, each 328 × 328 pixels corresponding to 1 km–by–1 km ground spacing, where 10% was used for validation, 10% as test dataset, and 80% for training the model.

Mapping tree cover and height using deep learning

We used the U-Net architecture (*46*) with an EfficientNet-B4 backbone (*47*) for both the tree cover segmentation and the tree height regression tasks (fig. S10). The modified U-Net has proven to be able to delineate tree canopies in very high resolution imagery (*11*, *38*, *48*). EfficientNets have shown to perform well with small parameter size by a predesigned network depth, width, and resolution. Because we need to deploy our model to the continental scale at 3-m resolution, we chose the EfficientNet-B4 as the trade-offs between performance and predicting (training) time. A key objective of our work was to assess tree resources outside forests as accurately as possible, and the crown size of such trees is often just a few pixels in our PlanetScope imagery. In the decoder, we replaced the simple two convolutional layers in the U-Net by residual blocks (*49*), which have been demonstrated to improve the model performance for segmenting small objects (*50*). Furthermore, spatial and channel squeeze and excitation blocks were integrated in the decoder to build attention mechanisms (*51*). The deep learning framework is built on an open-source segmentation library (*52*).

Mismatches between aerial CHM and PlanetScope data were sometimes observed in forested areas, when the images were not acquired from the same date. These inconsistencies cumulatively

contribute to a substantial proportion of loss in the regression, resulting in an unstable training progress and large uncertainties in the tree height estimations. Therefore, we first segmented the tree canopies, which were then used to mask the non-forested areas for minimizing the regression loss (fig. S10).

Tree crown segmentation

We set a 3-m height threshold to the aerial CHM data and converted it into a reference binary (tree or background) map. The four-band input data from PlanetScope were augmented by random cropping, flipping, and brightness distortion and then normalized channel-wise based on training dataset statistics before feeding into the model. We used the focal Tversky loss (*53*) as loss function for the segmentation model, and the alpha and beta parameters in the Tversky index (*54*) penalizing false positives and false negatives were set to 0.4 and 0.6, respectively. The focal parameter was set to 1.2, which incentivizes the model to focus on harder examples (when the Tversky index < 0.5), especially for the cases where scattered trees or tree lines do not exactly overlap between PlanetScope and aerial CHM data. We used Adam (*55*) as optimizer with an initial learning rate of 0.0001 and then reduced the learning rate by a factor of 0.1 when the metric has stopped improving for 30 epochs. Model training stopped when the learning rate reached 1×10^{-7}. In our study, each epoch of training took approximately 0.5 hour on a GeForce RTX 3090 GPU. The model achieved convergence after 180 epochs. Subsequently, the trained model was then used to predict a binary tree/non-tree cover map at 3-m for the entire study area. Notably, for each tile (1° by 1°), the prediction process took only 3 to 5 min.

Tree height regression

We used the same network architecture and training strategy as for the segmentation task, with an inverse sample–frequency weighting smooth–L1 loss function to mitigate the underestimation that is often observed for tall trees (*26*). The regression loss was only calculated for areas that overlap between the segmentation tree mask and the aerial CHM (>3 m). While this largely eliminated uncertainties from mismatches between the two data sources, the model still underestimated taller forests, possibly resulting from unclear training data. For example, coniferous forests vary optically only little in PlanetScope image but can have different heights in the CHM, depending on their location. As a consequence, whenever the model encounters this situation, it conservatively predicts intermediate values. One solution is to encode geo-information into the model (*50*) or include as input data (*26*). However, this would require a more homogeneous distribution of the reference data. We thus included a GEDI/Sentinel-2–based height map from (*26*) as auxiliary data (additional input band) to provide prior knowledge to the model about the forested areas, resulting in a total of five bands for the tree height regression task. For the regression task, both the training and prediction times are comparable to tree segmentation. However, the model required a longer time to converge.

Allometry for biomass estimation

Allometric equations provide aboveground biomass estimates from related tree measurements, such as stem diameter at breast height, canopy height, or crown diameter (*56*). We associated plot-level biomass derived from species-specific equations and field measured stem diameters with airborne LiDAR CHM (>1.3 m) averaged over the same plots (*56*, *57*). The plot-based aboveground biomass includes trees of all sizes above 1.3 m including understory, and relating the total aboveground biomass value per plot with the average canopy height derived from airborne LiDAR (for all areas with woody vegetation > 1.3 m, following the NFI definition) automatically corrects for the bias from undetectable understory. The regression equation in the log-log space can be described as

$$\ln(\mathrm{AGBD}) = \alpha + \beta \times \ln(\mathrm{H}) + \varepsilon \quad (1)$$

where AGBD is the aboveground biomass density (in kilograms per square meter), H is the average canopy height for woody vegetation taller than 1.3 m for the NFI plot area from the aerial CHM, α and β are the regression coefficients, and ε is normally distributed error term with zero mean and standard deviation σ, that is, $\varepsilon \sim N(0, \sigma^2)$. When back-transforming Eq. 1, we corrected for logarithmic bias using the Baskerville correction (*58*).

Plot-level biomass data were from the Danish NFI (n = 11,296) collected between 2012 and 2021 (*31*). Each plot was a circle with a radius of 15 m, where averaged tree height, estimated aboveground biomass, and forest fraction were provided. To remove misaligned plots, we filtered plots where the forest cover difference was more than 30% but kept data regardless of the collection year, assuming that dynamics are averaged out by the large number of plots. We derived forest-type–specific relationships using the Copernicus forest map from 2018 (*32*) to classify the plots in broadleaved forest (bf), coniferous forest (cf), mixed forest (mf), and areas of sparse tree cover (nf), which are plots that fall outside of the areas mapped as forest in the Copernicus forest-type map (fig. S6). We acknowledge that the class representing the non-forest trees (nf) is not ideal, because the Danish NFI does not systematically measure trees outside forests and other wooded lands. However, here, we assume that plots being located in areas of sparse tree cover and having a low biomass are most representative for non-forest areas. Because the NFI biomass data include all trees taller 1.3 m and not only those visible from an aerial perspective and in the PlanetScope images (typically >3-m height and 10-m^2 crown size), the different relationships include understory or small trees, which indirectly correct for the bias of missing small trees in the PlanetScope-based tree height predictions. This fact makes it important to have a separated equation for trees outside forests, which typically have a lower amount of understory. The equations and the number of NFI plots are as follows

$$\mathrm{AGBD_{bf}} = \exp[-2.427] \times \mathrm{H}^{1.794} \times \exp[0.134^2/2] \quad (N_{\mathrm{bf}} = 7232) \quad (2)$$

$$\mathrm{AGBD_{cf}} = \exp[-1.652] \times \mathrm{H}^{1.547} \times \exp[0.152^2/2] \quad (N_{\mathrm{cf}} = 3768) \quad (3)$$

$$\mathrm{AGBD_{mf}} = \exp[-2.243] \times \mathrm{H}^{1.728} \times \exp[0.118^2/2] \quad (N_{\mathrm{mf}} = 7536) \quad (4)$$

$$\mathrm{AGBD_{nf}} = \exp[-2.227] \times \mathrm{H}^{1.742} \times \exp[0.305^2/2] \quad (N_{\mathrm{nf}} = 409) \quad (5)$$

We used 20% of the plots randomly selected for each type to derive error metrics shown in fig. S6. Overall, the equations

showed a reasonable performance with a relative low bias (averaged R^2 = 0.62, bias = −8.7%, and RMSE = 5.43 kg/m^2).

Plot-level aboveground biomass in kg was then estimated as

$$\mathrm{AGB} = (\mathrm{TCP}/100) \times 900 \times \mathrm{AGBD} \quad (6)$$

where TCP is predicted tree cover percentage aggregated in 30 m–by–30 m resolution (rasterized NFI plot size). AGBD is obtained from Eqs. 2 to 5 according to the dominant forest type within the plot area. The aboveground biomass at 30-m resolution was lastly aggregated to the hectare level, containing both forest and non-forest information (Fig. 4).

Evaluation

We randomly selected 10% of the CHM dataset (10,000 1 km–by–1 km samples) as independent test dataset, which was not used for training and to optimize the model parameters during training, neither for the tree cover segmentation nor for the tree height regression tasks. We evaluated our results at pixel level (3 m by 3 m) using the intersection over union (IoU), which quantifies how well the predicted boundaries align with the ground truth boundaries, for the segmentation and the RMSE for tree height regression and aggregated to 1 km–by–1 km grids using the relative systematic error (bias %, Eq. 7); positive bias represents an overall overestimation, and negative bias represents an overall underestimation (*56*)

$$\mathrm{bias} = \frac{1}{N}\sum_{i=1}^{N}\left(\frac{Y_{\mathrm{pred}} - Y_{\mathrm{true}}}{Y_{\mathrm{true}}}\right) \times 100 \quad (7)$$

and the rRMSE in percentage described in Eq. 8

$$\mathrm{rRMSE} = \sqrt{\frac{1}{N}\sum_{i=1}^{N}\left(\frac{Y_{\mathrm{true}} - Y_{\mathrm{pred}}}{Y_{\mathrm{true}}}\right)^2} \times 100 \quad (8)$$

Tree cover segmentation

Overall, our model achieved an IoU of 0.692 on the test dataset (n = 10,000 plots of 1 km by 1 km). Further evaluation revealed a good alignment between our tree cover map and the tree cover map from aerial CHM data (using a 3-m height threshold) with overall R^2 values of 0.92 but with variation across biomes (fig. S2E). Trees can be segmented more precisely in both boreal (R^2 = 0.97, bias = −1.0%, and rRMSE = 13.5%) and temperate zones (R^2 = 0.99, bias = −0.8%, and rRMSE = 18.5%) than in the Mediterranean zone (R^2 = 0.39, bias = −8.2%, and rRMSE = 89.8%), which is likely due to two reasons: First, a limited amount of training data was usable from Spain because of the large temporal gap between PlanetScope imagery and the available aerial CHM data, which is from 2012. Second, the method of using a constant height threshold to generate the tree mask is not fully functional in diverse vegetation structures consisting of trees and shrubs. For areas with trees outside forest, our predictions compared with aerial CHM data achieve an overall bias = −2.4% and rRMSE = 36.6% (fig. S3 and Fig. 2D). We also calculated a confusion matrix comparing Danish NFI plots (n = 13,638) classified as either forest or no forest with our data following the FAO definition, showing a very high agreement with an overall accuracy of 0.96 (fig. 7A).

Tree height regression

We evaluated our tree height model by a residual analysis between reference height from the test dataset and the corresponding predicted tree height at pixel level (3-m resolution) (Fig. 2A). The model performance varied across biomes and canopy height ranges yet was closely related to the data distribution (Fig. 2B). In general, the model did not show a considerable saturation for taller canopies, yielding an RMSE of 5.4 m and an mean absolute error of 4.2 m. We found similar metrics as for the segmentation across biomes at plot-level evaluation, with R^2 = 0.82, bias = −2.4%, and rRMSE = 17.9% for the boreal zone; R^2 = 0.9, bias = −1.6%, and rRMSE = 14.5% for the temperate zone; and R^2 = 0.45, bias = −20.1%, and rRMSE = 35.4% for the Mediterranean zone (fig. S2D). All slopes below the diagonal line indicated a slight underestimation, consistent with the pixel-level evaluation (Fig. 2A). As for trees outside forests, we obtained a bias of −1.6% and rRMSE of 26.4% (fig. S3A). We further evaluated our top height estimation with field measured plot scale height from Danish NFI data (n = 3451) (fig. S7B), showing an underestimation bias of 9%.

North America

To test the generalization of our model, we then predicted tree cover and height for the boreal and temperate zone of North America and compared the results to aerial CHMs that were not used for either training or validation of the model parameters. Here, we acquired around 1000 km^2 of airborne LiDAR CHMs at 1-m resolution from (*59*) and generated 1036 samples with 1 km–by–1 km ground spacing following the same data processing procedure as described in the previous section. These evaluations show that our model can be deployed to a comparable landscape without a considerable loss of performance (R^2 = 0.71, bias = −15.7%, and rRMSE = 20% for height regression; and R^2 = 0.88, bias = +2%, and rRMSE = 28.6% for tree segmentation) (Fig. 6).

Evaluation of the allometry

We used NFI data from Spain (fig. S13), mostly located in the region of Extremadura (768 plots) measured in 2016 and 2017, and the province of Leon in the northwestern part of Spain (1162 plots), measured in 2019. The Spanish NFI measurements represent an important remeasurement campaign on which existing NFI plot locations have been remeasured with upgraded global navigation satellite system equipment to improve the geolocation of plot centers in existing and new plots (*60*). Airborne laser scanning data were collected in Leon from October 2019 to May 2020 and in Extremadura from October 2018 to July 2019, which largely match with the NFI measurements. In addition, we used 1284 plots that include a diverse mosaic of Mediterranean evergreen and broadleaf forests (*61*). We implemented the same procedure as applied in Denmark, to derive allometric equations using only the Spanish NFI data

$$\mathrm{AGBD_{bf}} = \exp[-3.1218] \times \mathrm{H}^{2.072} \times \exp[0.289^2/2] \quad (N_{\mathrm{bf}} = 2213) \quad (9)$$

$$\mathrm{AGBD_{cf}} = \exp[-2.161] \times \mathrm{H}^{1.693} \times \exp[0.294^2/2] \quad (N_{\mathrm{cf}} = 506) \quad (10)$$

$$\mathrm{AGBD_{nf}} = \exp[-1.608] \times \mathrm{H}^{1.479} \times \exp[0.446^2/2] \quad (N_{\mathrm{nf}} = 397) \quad (11)$$

Using these equations, we estimate 1120.7 Tg biomass for Spain, which is very close to the estimates using the equations from the Danish NFI data (1139.8 Tg). This consistency gives confidence

in the robustness and ability to generalize our allometric models, which were originally developed and validated in Denmark.

Biomass estimations

The errors from canopy cover, height, and the allometric equations propagate to the final biomass estimation, so we evaluated the uncertainty on the biomass maps in three ways. First, we compared the predicted biomass at field plot level with estimations from the Danish NFI for 3451 selected plots, resulting in an overall bias of −23% (fig. S7C). Because NFI data were collected in forest areas, this error is affected by the underestimation of very tall trees, where biomass densities can reach 300 Mg/ha (fig. S7C) and possible geolocation uncertainties between the PlanetScope images and the NFI plot locations recorded by a handheld GPS. Second, we compared our biomass estimation with other global biomass products (*27*, *28*, *33*). The GEDI biomass product (*33*) does not cover our entire research area, so we randomly sampled 4000 points (fig. S8), resulting in a bias of 1.8%. The biomass map from (*28*) shows good correlation with ours but with a higher bias (bias = 11.3% and r = 0.83). The biomass map from (*27*) shows an overall underestimation (bias = −37.9% and r = 0.82). Third, we further compared the PlanetScope-based biomass maps aggregated to the national scale with FAO country statistics (Fig. 5D and fig. S9A) (*5*): The overall bias over all 30 countries was 7.6%. Our biomass estimates reached similar levels but were slightly higher than the FAO statistics for most countries, which could result from trees outside forests that are typically not included in national inventory reports. The total bias for (*28*) and (*27*) at the country scale was calculated as +17.3 and +49.9%.

Environmental and auxiliary data

We used a GLCLU map from 2019 at 30 m (*30*) including forests, urban areas, cropland, and grassland to analyze trees outside forests and trees in different landscapes. We also used global canopy height products based on Sentinel-2 from 2020 at 10-m resolution (*26*) and another product based on Landsat from 2019 at 30-m resolution (*24*) for comparison. Both products use GEDI spaceborne canopy height data that were extrapolated with Sentinel-2 and Landsat, respectively. The GEDI/Sentinel-2–based canopy height map was also used to assist the height regression task. The Copernicus forest-type map based on Sentinel-2 data from 2018 at 10-m resolution and a PROBA-V–based forest-type map from 2019 at 100 m (*32*) were used to separate forests into coniferous and broadleaved forest across Europe. We further used the GEDI L4B biomass density product from 2020 available at 1-km resolution (*33*) and state-of-the-art global biomass density products from 2017 (*28*) and 2020 (*27*) at 100 m for biomass comparisons. We used biome data from (*62*) aggregated into three main biome zones (fig. S2).

Supplementary Materials

This PDF file includes:

Figs. S1 to S13
Table S1
References

REFERENCES AND NOTES

1. J.-F. Bastin, Y. Finegold, C. Garcia, D. Mollicone, M. Rezende, D. Routh, C. M. Zohner, T. W. Crowther, The global tree restoration potential. *Science* **365**, 76–79 (2019).
2. G. Ceccherini, G. Duveiller, G. Grassi, G. Lemoine, V. Avitabile, R. Pilli, A. Cescatti, Abrupt increase in harvested forest area over Europe after 2015. *Nature* **583**, 72–77 (2020).
3. C. Senf, R. Seidl, Mapping the forest disturbance regimes of Europe. *Nat. Sustain.* **4**, 63–70 (2021).
4. N. T. Hoang, K. Kanemoto, Mapping the deforestation footprint of nations reveals growing threat to tropical forests. *Nature Ecology & Evolution* **5**, 845–853 (2021).
5. "State of Europe's forests 2020 report" (Forest Europe, 2020).
6. A. Kangas, R. Astrup, J. Breidenbach, J. Fridman, T. Gobakken, K. T. Korhonen, M. Maltamo, M. Nilsson, T. Nord-Larsen, E. Næsset, H. Olsson, Remote sensing and forest inventories in Nordic countries–Roadmap for the future. *Scand. J. For. Res.* **33**, 397–412 (2018).
7. S. Magnussen, N.-L. Thomas, R.-N. Torben, Lidar supported estimators of wood volume and above-ground biomass from the Danish national forest inventory (2012–2016). *Remote Sens. Environ.* **211**, 146–153 (2018).
8. J. Breidenbach, A. Granhus, G. Hylen, R. Eriksen, R. Astrup, A century of National Forest Inventory in Norway–informing past, present, and future decisions. *For. Ecosyst.* **7**, 46 (2020).
9. E. Tomppo, H. Olsson, G. Ståhl, M. Nilsson, O. Hagner, M. Katila, Combining national forest inventory field plots and remote sensing data for forest databases. *Remote Sens. Environ.* **112**, 1982–1999 (2008).
10. J. A. Blackard, M. V. Finco, E. H. Helmer, G. Holden, M. Hoppus, D. M. Jacobs, A. J. Lister, G. G. Moisen, M. D. Nelson, R. Riemann, B. Ruefenacht, D. Salajanu, D. Weyermann, K. C. Winterberger, T. J. Brandeis, R. Czaplewski, R. E. Mc Roberts, P. L. Patterson, R. P. Tycio, Mapping U.S. forest biomass using nationwide forest inventory data and moderate resolution information. *Remote Sens. Environ.* **112**, 1658–1677 (2008).
11. M. Brandt, C. J. Tucker, A. Kariryaa, K. Rasmussen, C. Abel, J. Small, J. Chave, L. V. Rasmussen, P. Hiernaux, A. A. Diouf, L. Kergoat, O. Mertz, C. Igel, F. Gieseke, J. Schöning, S. Li, K. Melocik, J. Meyer, S. Sinno, E. Romero, E. Glennie, A. Montagu, M. Dendoncker, R. Fensholt, An unexpectedly large count of trees in the West African Sahara and Sahel. *Nature* **587**, 78–82 (2020).
12. S. Schnell, C. Kleinn, G. Ståhl, Monitoring trees outside forests: A review. *Environ. Monit. Assess.* **187**, 1–17 (2015).
13. N. Thomas, P. Baltezar, D. Lagomasino, A. Stovall, Z. Iqbal, L. Fatoyinbo, Trees outside forests are an underestimated resource in a country with low forest cover. *Sci. Rep.* **11**, 1–13 (2021).
14. J. Reed, J. van Vianen, S. Foli, J. Clendenning, K. Yang, M. MacDonald, G. Petrokofsky, C. Padoch, T. Sunderland, Trees for life: The ecosystem service contribution of trees to food production and livelihoods in the tropics. *For. Policy Econ.* **84**, 62–71 (2017).
15. R. J. Zomer, H. Neufeldt, J. Xu, A. Ahrends, D. Bossio, A. Trabucco, M. van Noordwijk, M. Wang, Global tree cover and biomass carbon on agricultural land: The contribution of agroforestry to global and national carbon budgets. *Sci. Rep.* **6**, 29987 (2016).
16. S. Schnell, D. Altrell, G. Ståhl, C. Kleinn, The contribution of trees outside forests to national tree biomass and carbon stocks—A comparative study across three continents. *Environ. Monit. Assess.* **187**, 1–18 (2015).
17. "Tree cover outside woodland in Great Britain report" (National Forest Inventory, 2017).
18. M. W. Thornton, P. M. Atkinson, D. A. Holland, Sub-pixel mapping of rural land cover objects from fine spatial resolution satellite sensor imagery using super-resolution pixel-swapping. *Int. J. Remote Sens.* **27**, 473–491 (2006).
19. D. Zanaga, R. Van De Kerchove, D. Daems, W. De Keersmaecker, C. Brockmann, G. Kirches, J. Wevers, O. Cartus, M. Santoro, S. Fritz, M. Lesiv, M. Herold, N.-E. Tsendbazar, P. Xu, F. Ramoino, O. Arino, ESA WorldCover 10 m 2021 v200 (2022); https://zenodo.org/record/7254221.
20. M. C. Hansen, P. V. Potapov, R. Moore, M. Hancher, S. A. Turubanova, A. Tyukavina, D. Thau, S. V. Stehman, S. J. Goetz, T. R. Loveland, A. Kommareddy, A. Egorov, L. Chini, C. O. Justice, J. R. G. Townshend, High-resolution global maps of 21st-century forest cover change. *Science* **342**, 850–853 (2013).
21. FAO, FAOSTAT, "Food and agriculture organization of the United Nations, Rome, Italy" (2018).
22. C. Alexander, P. K. Bøcher, L. Arge, J. C. Svenning, Regional-scale mapping of tree cover, height and main phenological tree types using airborne laser scanning data. *Remote Sens. Environ.* **147**, 156–172 (2014).
23. E. Malkoç, M. Rüetschi, C. Ginzler, L. T. Waser, Countrywide mapping of trees outside forests based on remote sensing data in Switzerland. *Int. J. Appl. Earth Obs. Geoinf.* **100**, 102336 (2021).
24. P. Potapov, X. Li, A. Hernandez-Serna, A. Tyukavina, M. C. Hansen, A. Kommareddy, A. Pickens, S. Turubanova, H. Tang, C. E. Silva, J. Armston, R. Dubayah, J. B. Blair, M. Hofton, Mapping global forest canopy height through integration of GEDI and Landsat data. *Remote Sens. Environ.* **253**, 112165 (2021).

25. N. Lang, N. Kalischek, J. Armston, K. Schindler, R. Dubayah, J. D. Wegner, Global canopy height regression and uncertainty estimation from GEDI LIDAR waveforms with deep ensembles. *Remote Sens. Environ.* **268**, 112760 (2022).
26. N. Lang, W. Jetz, K. Schindler, J. D. Wegner, A high-resolution canopy height model of the Earth. arXiv:2204.08322 (2022); https://doi.org/10.48550/arXiv.2204.08322.
27. L. Xu, S. S. Saatchi, Y. Yang, Y. Yu, J. Pongratz, A. A. Bloom, K. Bowman, J. Worden, J. Liu, Y. Yin, G. Domke, R. E. McRoberts, C. Woodall, G.-J. Nabuurs, S. de-Miguel, M. Keller, N. Harris, S. Maxwell, D. Schimel, Changes in global terrestrial live biomass over the 21st century. *Sci. Adv.* **7**, eabe9829 (2021).
28. M. Santoro, O. Cartus, N. Carvalhais, D. M. A. Rozendaal, V. Avitabile, A. Araza, S. de Bruin, M. Herold, S. Quegan, P. Rodríguez-Veiga, H. Balzter, J. Carreiras, D. Schepaschenko, M. Korets, M. Shimada, T. Itoh, Á. Moreno Martínez, J. Cavlovic, R. Cazzolla Gatti, P. da Conceição Bispo, N. Dewnath, N. Labrière, J. Liang, J. Lindsell, E. T. A. Mitchard, A. Morel, A. M. Pacheco Pascagaza, C. M. Ryan, F. Slik, G. Vaglio Laurin, H. Verbeeck, A. Wijaya, S. Willcock, The global forest above-ground biomass pool for 2010 estimated from high-resolution satellite observations. *Earth Syst. Sci. Data* **13**, 3927–3950 (2021).
29. D. J. Luscombe, N. Gatis, K. Anderson, D. Carless, R. E. Brazier, Rapid, repeatable landscape-scale mapping of tree, hedgerow, and woodland habitats (THaW), using airborne LiDAR and spaceborne SAR data. *Ecol. Evol.* **13**, e10103 (2023).
30. M. C. Hansen, P. V. Potapov, A. H. Pickens, A. Tyukavina, A. Hernandez-Serna, V. Zalles, S. Turubanova, I. Kommareddy, S. V. Stehman, X. P. Song, A. Kommareddy, Global land use extent and dispersion within natural land cover using Landsat data. *Environ. Res. Lett.* **17**, 034050 (2022).
31. T. Nord-Larsen, V. K. Johannsen, T. Riis-Nielsen, I. M. Thomsen, B. B. Jørgensen, "Skovstatistik 2019: Forest statistics 2019" (Institut for Geovidenskab og Naturforvaltning, Københavns Universitet, 2020).
32. European Environment Agency, Copernicus Land Monitoring Service (2018).
33. R. O. Dubayah, J. Armston, S. P. Healey, Z. Yang, P. L. Patterson, S. Saarela, G. Stahl, L. Duncanson, J. R. Kellner, "GEDI L4B Gridded Aboveground Biomass Density, Version 2" (ORNL DAAC, 2022).
34. C. Tucker, M. Brandt, P. Hiernaux, A. Kariryaa, K. Rasmussen, J. Small, C. Igel, F. Reiner, K. Melocik, J. Meyer, S. Sinno, E. Romero, E. Glennie, Y. Fitts, A. Morin, J. Pinzon, D. McClain, P. Morin, C. Porter, S. Loeffler, L. Kergoat, B. A. Issoufou, P. Savadogo, J. P. Wigneron, B. Poulter, P. Ciais, R. Kaufmann, R. Myneni, S. Saatchi, R. Fensholt, Sub-continental-scale carbon stocks of individual trees in African drylands. *Nature* **615**, 80–86 (2023).
35. R. Dubayah, J. B. Blair, S. Goetz, L. Fatoyinbo, M. Hansen, S. Healey, M. Hofton, G. Hurtt, J. Kellner, S. Luthcke, J. Armston, H. Tang, L. Duncanson, S. Hancock, P. Jantz, S. Marselis, P. L. Patterson, W. Qi, C. Silva, The Global Ecosystem Dynamics Investigation: High-resolution laser ranging of the Earth's forests and topography. *Sci. Remote Sens.* **1**, 100002 (2020).
36. S. Quegan, T. le Toan, J. Chave, J. Dall, J. F. Exbrayat, D. H. T. Minh, M. Lomas, M. M. D'Alessandro, P. Paillou, K. Papathanassiou, F. Rocca, S. Saatchi, K. Scipal, H. Shugart, T. L. Smallman, M. J. Soja, S. Tebaldini, L. Ulander, L. Villard, M. Williams, The European Space Agency BIOMASS mission: Measuring forest above-ground biomass from space. *Remote Sens. Environ.* **227**, 44–60 (2019).
37. Y. Cheng, A. Vrieling, F. Fava, M. Meroni, M. Marshall, S. Gachoki, Phenology of short vegetation cycles in a Kenyan rangeland from PlanetScope and Sentinel-2. *Remote Sens. Environ.* **248**, 112004 (2020).
38. F. Reiner, M. Brandt, X. Tong, D. Skole, A. Kariryaa, P. Ciais, A. Davies, P. Hiernaux, J. Chave, M. Mugabowindekwe, C. Igel, S. Oehmcke, F. Gieseke, S. Li, S. Liu, S. Saatchi, P. Boucher, J. Singh, S. Taugourdeau, M. Dendoncker, X.-P. Song, O. Mertz, C. J. Tucker, R. Fensholt, More than one quarter of Africa's tree cover found outside areas previously classified as forest. *Nat. Commun.* **14**, 2258 (2022).
39. S. Li, M. Brandt, R. Fensholt, A. Kariryaa, C. Igel, F. Gieseke, T. Nord-Larsen, S. Oehmke, A. Holm-Carlsen, S. Junttila, X. Tong, Alexandre d'Aspremont, P. Ciais, Digital twinning of all forest and non-forest trees at national level via deep learning. (2022) 10.21203/rs.3.rs-1661442/v1.
40. "Woodland cover target: detailed evidence report" (Department for Environment, Food and Rural Affairs, 2022).
41. "The sixth carbon budget: The UK's path to net zero" (The Climate Change Committee, 2020).
42. M. Friedl, J. Gray, D. Sulla-Menashe, "MCD12Q2 MODIS/Terra+ aqua land cover dynamics yearly L3 global 500m SIN Grid V006. NASA EOSDIS land processes DAAC" (2019).
43. LAStools, Efficient LiDAR processing software (version 141017, academic); http://rapidlasso.com/LAStools.
44. Microsoft Building Footprints; https://github.com/microsoft/GlobalMLBuildingFootprints.
45. OpenStreetMap contributors, Planet dump building footprint database (2015); https://planet.openstreetmap.org.
46. O. Ronneberger, P. Fischer, T. Brox, "U-net: Convolutional networks for biomedical image segmentation," in *International Conference on Medical Image Computing and Computer-Assisted Intervention (MICCAI)* (Springer, 2015).
47. M. Tan, L. Quoc, "EfficientNet: Rethinking model scaling for convolutional neural networks" in *Proceedings of Machine Learning Research* (PMLR) (ML Research Press, 2019).
48. M. Mugabowindekwe, M. Brandt, J. Chave, F. Reiner, D. L. Skole, A. Kariryaa, C. Igel, P. Hiernaux, P. Ciais, O. Mertz, X. Tong, S. Li, G. Rwanyiziri, T. Dushimiyimana, A. Ndoli, V. Uwizeyimana, J.-P. B. Lillesø, F. Gieseke, C. J. Tucker, S. Saatchi, R. Fensholt, Nation-wide mapping of tree-level aboveground carbon stocks in Rwanda. *Nat. Clim. Chang* **13**, 91–97 (2022).
49. K. He, X. Zhang, S. Ren, J. Sun, Deep residual learning for image recognition. arXiv:1512.03385 (2016); https://doi.org/10.48550/arXiv.1512.03385.
50. W. Sirko, S. Kashubin, M. Ritter, A. Annkah, Yasser Salah Eddine Bouchareb, Y. Dauphin, D. Keysers, M. Neumann, M. Cisse, J. Quinn, Continental-scale building detection from high resolution satellite imagery. arXiv:2107.12283 (2021); https://doi.org/10.48550/arXiv.2107.12283.
51. A. G. Roy, N. Navab, C. Wachinger, "Concurrent spatial and channel 'squeeze & excitation'in fully convolutional networks," in *International Conference on Medical Image Computing and Computer-Assisted Intervention* (Springer, 2018).
52. Pavel Iakubovskii, et al. Segmentaton Models Pytorch; https://github.com/qubvel/segmentation_models.pytorch (2019).
53. N. Abraham, N. M. Khan, "A novel focal Tversky loss function with improved attention u-net for lesion segmentation," *2019 IEEE 16th International Symposium on Biomedical Imaging*, Venice, Italy, 8 to 11 April 2019).
54. A. Tversky, Features of similarity. *Psychol. Rev.* **84**, 327–352 (1977).
55. D. P. Kingma, J. Ba, "Adam: A method for stochastic optimization," *Proceedings of the 3rd International Conference on Learning Representations* (ICLR), San Diego, CA, 7 to 9 May 2015).
56. T. Jucker, J. Caspersen, J. Chave, C. Antin, N. Barbier, F. Bongers, M. Dalponte, K. Y. van Ewijk, D. I. Forrester, M. Haeni, S. I. Higgins, R. J. Holdaway, Y. Iida, C. Lorimer, P. L. Marshall, S. Momo, G. R. Moncrieff, P. Ploton, L. Poorter, K. A. Rahman, M. Schlund, B. Sonké, F. J. Sterck, A. T. Trugman, V. A. Usoltsev, M. C. Vanderwel, P. Waldner, B. M. M. Wedeux, C. Wirth, H. Wöll, M. Woods, W. Xiang, N. E. Zimmermann, D. A. Coomes, Allometric equations for integrating remote sensing imagery into forest monitoring programmes. *Glob. Chang. Biol.* **23**, 177–190 (2017).
57. N. P. Hanan, L. Prihodko, C. W. Ross, G. Bucini, A. T. Tredennick, "Gridded estimates of woody cover and biomass across Sub-Saharan Africa, 2000–2004" (ORNL DAAC, 2020); https://doi.org/10.3334/ORNLDAAC/1777.
58. G. L. Baskerville, Use of logarithmic regression in the estimation of plant biomass. *Can. J. For. Res.* **2**, 49–53 (1972).
59. B. D. Cook, L. A. Corp, R. F. Nelson, E. M. Middleton, D. C. Morton, J. T. McCorkel, J. G. Masek, K. J. Ranson, V. Ly, P. M. Montesano, NASA Goddard's LiDar, hyperspectral and thermal (G-LiHT) airborne imager. *Remote Sens. (Basel)* **5**, 4045–4066 (2013).
60. A. Pascual, J. Guerra-Hernández, D. N. Cosenza, V. Sandoval-Altelarrea, Using enhanced data co-registration to update Spanish National Forest Inventories (NFI) and to reduce training data under LiDAR-assisted inference. *Int. J. Remote Sens.* **42**, 126–147 (2021).
61. A. Pascual, J. Guerra-Hernández, J. Armston, D. M. Minor, L. I. Duncanson, P. B. May, J. R. Kellner, R. Dubayah, Assessing the performance of NASA's GEDI L4A footprint aboveground biomass density models using National Forest Inventory and airborne laser scanning data in Mediterranean forest ecosystems. *For. Ecol. Manage.* **538**, 120975 (2023).
62. E. Dinerstein, D. Olson, A. Joshi, C. Vynne, N. D. Burgess, E. Wikramanayake, N. Hahn, S. Palminteri, P. Hedao, R. Noss, M. Hansen, H. Locke, E. C. Ellis, B. Jones, C. V. Barber, R. Hayes, C. Kormos, V. Martin, E. Crist, W. Sechrest, L. Price, J. E. M. Baillie, D. Weeden, K. Suckling, C. Davis, N. Sizer, R. Moore, D. Thau, T. Birch, P. Potapov, S. Turubanova, A. Tyukavina, N. de Souza, L. Pintea, J. C. Brito, O. A. Llewellyn, A. G. Miller, A. Patzelt, S. A. Ghazanfar, J. Timberlake, H. Klöser, Y. Shennan-Farpón, R. Kindt, J. P. B. Lillesø, P. van Breugel, L. Graudal, M. Voge, K. F. al-Shammari, M. Saleem, An ecoregion-based approach to protecting half the terrestrial realm. *Bioscience* **67**, 534–545 (2017).
63. *IPCC Guidelines for National Greenhouse Gas Inventories* (IPCC, 2006).

Acknowledgments

Funding: This research was supported by the European Research Council (ERC) under the European Union's Horizon 2020 research and innovation programme (grant agreement no. 947757 TOFDRY) and a DFF Sapere Aude grant (no. 9064–00049B). S. Liu is funded by China Scholarship Council (CSC; grant no. 202104910123). R.F., C.I., and N.L. acknowledge support by the Villum Fonden through the project Deep Learning and Remote Sensing for Unlocking Global Ecosystem Resource Dynamics (DeReEco; grant no. 34306). C.I. acknowledges support by the Pioneer Centre for AI, DNRF grant number P1. Y.Y. and M.B. acknowledge support by the International Partnership Program of Chinese Academy of Sciences (CAS) (092GJHZ2022029GC) and CAS Interdisciplinary Team (JCTD-2021-16). J.G. acknowledges support by Foundation for

Science and Technology (FCT) through a CEEC contract (CEECIND/02576/2002). **Author contributions:** M.B., R.F., and S. Liu designed the study. M.B. prepared and processed the aerial LiDAR CHM data. T.N.-L. provided Danish NFI data. A.P. and J.G.-H. provided Spanish NFI data. F.R. and X.T. developed the code for the PlanetScope imagery generation pipeline. J.C. designed the biomass allometry, implemented by S. Liu, N.L., C.I., S. Li, M.M. S. Liu wrote the code for the deep learning framework, supported by F.R., S. Li, and Z.C. Interpretations were done by M.B., S. Liu, N.L., P.C., J.C., C.I., S.S., Y.Y., R.F., and S. Liu conducted the analyses. S. Liu and M.B. wrote the first manuscript draft with contributions by all authors. S. Liu designed the figures. **Competing interests:** The authors declare that they have no competing interests. **Data and materials availability:** All data needed to evaluate the conclusions in the paper are present in the paper and/or the Supplementary Materials. PlanetScope imagery was purchased via a departmental license, and the images cannot be distributed. Derived products produced in this study: Canopy height, cover, and biomass maps across Europe have been deposited in the Zenodo database and are available at https://doi.org/10.5281/zenodo.8154445. Links to download the open LiDAR data can be found under https://publications.jrc.ec.europa.eu/repository/bitstream/JRC126223/jrc126223_jrc126223_lidaropensourcedata.pdf. The code for tree segmentation and height regression is built on publicly open-source framework Segmentation Models PyTorch, available at https://github.com/qubvel/segmentation_models.pytorch. Custom code is publicly available at https://doi.org/10.5281/zenodo.8156190.

Submitted 1 March 2023
Accepted 15 August 2023
Published 15 September 2023
10.1126/sciadv.adh4097

ScienceAdvances

The overlooked contribution of trees outside forests to tree cover and woody biomass across Europe

Siyu Liu, Martin Brandt, Thomas Nord-Larsen, Jerome Chave, Florian Reiner, Nico Lang, Xiaoye Tong, Philippe Ciais, Christian Igel, Adrian Pascual, Juan Guerra-Hernandez, Sizhuo Li, Maurice Mugabowindekwe, Sassan Saatchi, Yuemin Yue, Zhengchao Chen, and Rasmus Fensholt

Sci. Adv., **9** (37), eadh4097.
DOI: 10.1126/sciadv.adh4097